AGU PUBLICATIONS

JGR

Journal of Geophysical Research: Solid Earth

RESEARCH ARTICLE
10.1002/2015JB012073

Key Points:
- Convergence between African and Eurasia causes distributed deformation in the Alboran Sea
- Alboran seismicity outlines a 20–40 km wide NNE-SSW trending band of deformation
- Local earthquakes correlate with imaged fault, but some faults remained seismically inactive

Correspondence to:
I. Grevemeyer,
igrevemeyer@geomar.de

Citation:
Grevemeyer, I., E. Gràcia, A. Villaseñor, W. Leuchters, and A. B. Watts (2015), Seismicity and active tectonics in the Alboran Sea, Western Mediterranean: Constraints from an offshore-onshore seismological network and swath bathymetry data, *J. Geophys. Res. Solid Earth*, *120*, doi:10.1002/2015JB012073.

Received 27 MAR 2015
Accepted 30 OCT 2015
Accepted article online 3 NOV 2015

Seismicity and active tectonics in the Alboran Sea, Western Mediterranean: Constraints from an offshore-onshore seismological network and swath bathymetry data

Ingo Grevemeyer[1], Eulàlia Gràcia[2], Antonio Villaseñor[3], Wiebke Leuchters[1], and Anthony B. Watts[4]

[1]GEOMAR Helmholtz Centre of Ocean Research, Kiel, Germany, [2]Barcelona-Center for Subsurface Imaging, Institut de Ciències del Mar - CSIC Barcelona, Spain, [3]Institute of Earth Sciences Jaume Almera, ICTJA-CSIC, Barcelona, Spain, [4]Department of Earth Sciences, University of Oxford, UK

Abstract Seismicity and tectonic structure of the Alboran Sea were derived from a large amphibious seismological network deployed in the offshore basins and onshore in Spain and Morocco, an area where the convergence between the African and Eurasian plates causes distributed deformation. Crustal structure derived from local earthquake data suggests that the Alboran Sea is underlain by thinned continental crust with a mean thickness of about 20 km. During the 5 months of offshore network operation, a total of 229 local earthquakes were located within the Alboran Sea and neighboring areas. Earthquakes were generally crustal events, and in the offshore domain, most of them occurred at crustal levels of 2 to 15 km depth. Earthquakes in the Alboran Sea are poorly related to large-scale tectonic features and form a 20 to 40 km wide NNE-SSW trending belt of seismicity between Adra (Spain) and Al Hoceima (Morocco), supporting the case for a major left-lateral shear zone across the Alboran Sea. Such a shear zone is in accord with high-resolution bathymetric data and seismic reflection imaging, indicating a number of small active fault zones, some of which offset the seafloor, rather than supporting a well-defined discrete plate boundary fault. Moreover, a number of large faults known to be active as evidenced from bathymetry, seismic reflection, and paleoseismic data such as the Yusuf and Carboneras faults were seismically inactive. Earthquakes below the Western Alboran Basin occurred at 70 to 110 km depth and hence reflected intermediate depth seismicity related to subducted lithosphere.

1. Introduction

There is an increasing need for a better understanding of regional seismic and tsunami hazards, particularly in coastal and offshore domains, where the detailed structure of submarine faults is often unknown. Further, offshore seismicity is often based on epicenters derived from onshore networks and hence associated with large uncertainties. Therefore, it is generally difficult to establish a relationship between seismicity and active faults at sea, especially in areas where large destructive earthquakes may have a long recurrence interval, as at the Southern Iberian Margin and in the Alboran Sea, Western Mediterranean [*Instituto Geográfico Nacional*, 2013, http://www.ign.es/ign/resources/sismologia/publicaciones/CatalogoGeneralIsosistas.pdf; *Keller et al*., 1995].

Seismotectonics of the Alboran Sea and adjacent continents is controlled by the NW-SE trending convergence (4.3 +/− 0.5 mm/yr) between the African and Eurasian plates [e.g., *McClusky et al*., 2003, *De Mets et al*., 2010] and mantle forcing caused by the remaining slab of subducted lithosphere beneath the West Alboran Basin [e.g., *Perouse et al*., 2010; *Pedrera et al*., 2011; *García-Castellanos and Villaseñor*, 2011; *Bezada et al*., 2013], causing widespread earthquake activity and seismic hazards in southern Iberia [e.g., *Gràcia et al*., 2003; 2006; *Buforn et al*., 2004; *Marín-Lechado et al*., 2005]. However, the existence and exact location of a discrete African-Eurasian plate boundary is still a matter of debate.

To the east of the Alboran Sea along the northern Algerian margin, the African-Eurasian plate boundary corresponds to a narrow band of well-defined shallow seismicity (<30 km depth) [e.g., *Buforn et al*., 2004]. Focal mechanisms support thrust faulting with NW-SE trending fault planes [*Stich et al*., 2003a; *Meghraoui and Pondrelli*, 2012], in accordance with Eurasia and Africa plate convergence. In the Rif-Betic-Alboran domain, the plate boundary is more diffuse and probably distributed among different structures. *Stich et al*. [2003a] suggested that it may correspond to a NE-SW trending band of distributed seismicity from the Eastern Betic Shear Zone [*Bousquet*, 1979; *Sanz de Galdeano*, 1990], across the Alboran Sea, to the Rif, and

referred to as the Betic-Alboran Shear Zone [*De Larouzière et al*., 1988] or Trans-Alboran Shear Zone. Moment rate, slip velocity, and *b* values indicate that the strain accumulated in the region is partly released in a continuous seismic activity of moderate magnitude over the whole area [e.g., *Buforn et al*., 2004]. Earthquakes with magnitudes Mw = 6 may occur at prolonged intervals. The largest historic earthquakes had Medvedev-Sponheuer-Karnik (MSK) scale intensities of ~IX and include the 1522 Almería and the 1804 Dalías events with epicenters located offshore in the Alboran Sea [*Instituto Geográfico Nacional*, 2013, http://www.ign.es/ign/resources/sismologia/publicaciones/CatalogoGeneralIsosistas.pdf; *Keller et al*., 1995; *Reicherter and Hübscher*, 2007]. The most recent large earthquake was the MSK ~ VIII Adra earthquake of 1910 with an estimated moment magnitude of Mw = 6.1 [*Stich et al*., 2003b]. In the western Alboran Sea, intermediate depth earthquakes (40–150 km depth) are most likely related to a remaining slab [*García-Castellanos and Villaseñor*, 2011; *Ruiz-Constán et al*., 2011; *Bezada et al*., 2013] of stalled subduction [*Chertova et al*., 2014].

The relationship between morphological features in the Alboran Sea, like the Alboran Ridge and faults imaged in the bathymetry [e.g., *Gràcia et al*., 2006, 2012; *Ballesteros et al*., 2008; *Muñoz et al*., 2008; *Martínez-García et al*., 2011], the stress pattern and the distribution of earthquakes are still poorly known. Further, the maximum earthquake size is inherently related to the size of a fault zone. Thus, the thickness of the seismogenic layer (maximum depth of faulting) provides important constraints for assessment of geological hazards. To constrain earthquake distribution, stresses, and seismotectonics of the Alboran Sea and surrounding areas, we studied micro-earthquakes recorded with an extensive amphibious network of 30 ocean bottom seismometers (OBS) and 155 land stations in Spain and Morocco. Networks were operated within the framework of the European Science Foundation coordinated project TOPO-MED and the Spanish project TOPO-IBERIA, respectively, providing a unique data set of local earthquakes. Seismicity pattern will be discussed with respect to faults recently identified in bathymetric maps and imaged on seismic profiles.

2. Tectonic Setting

The Gibraltar Arc and Betic-Rif cordilleras constitute the westernmost end of the Mediterranean Alpine ranges at the boundary between the African and Eurasian plates. Slab rollback is now considered as the major process that during the last 25–30 Myr has been responsible for controlling the present shape of the Mediterranean region [*Royden*, 1993; *Faccenna et al*., 2001; *Mauffret et al*., 2004; *Sparkman and Wortel*, 2004; *Chertova et al*., 2014]. However, its role in the generation of the Alboran Sea, a Neogene extensional basin [e.g., *Watts et al*., 1993], is still controversial. Indeed, several geodynamical models have been proposed to explain the formation of the Alboran Sea simultaneously with compression and formation of the mountain chains of the Betics and Rif. These models variously explain the Alboran Basin as the consequence of the collapse of a thick lithospheric root [*Platt and Vissers*, 1989; *Calvert et al*., 2000], crustal extrusion due to forces transmitted across the Africa-Eurasia plate boundary [*Rebai et al*., 1992], or break-off of a subducting slab [*Blanco and Spakman*, 1993]. However, numerical simulations render the origin of the Alboran domain less controversial as a stretched continental fragment that originates from the Oligocene trench region at the Baleares margin that was dragged (and perhaps additionally stretched) to its present location in the wake of slab rollback [*van Hinsbergen et al*., 2014; *Chertova et al*., 2014].

Recent tomographic images clearly support the scenario of a westward retreating slab and subsequent formation of a back-arc basin [*Bezada et al*., 2013; *García-Castellanos and Villaseñor*, 2011; *Chertova et al*., 2014]. The slab, however, seems to be detached under the Betics [*Sparkman and Wortel*, 2004]. Geochemistry and dating of volcanic outcrops and constraints from Ocean Drilling Program (ODP) drilling indicates an immature volcanic arc crust in the eastern Alboran Sea formed 11 to 8 Myr ago [*Duggen et al*., 2003, 2004], in agreement with multichannel seismic imaging results [*Booth-Rea et al*., 2007].

Morphologically, the Alboran Sea can be separated into two main basins, the West Alboran Basin and the East Alboran Basin (Figure 1). The seafloor morphology is complex, made up of ridges, seamounts, faults, and deep basins. During ODP Leg 161 the West Alboran Basin basement was sampled, highlighting the presence of metamorphic rocks of continental origin rather than oceanic [e.g., *Comas et al*., 1999]. However, drilling in the East Alboran Basin recovered calc-alkaline to alkaline rocks [*Duggen et al*., 2003, 2004], supporting magmatic arc-type crust or continental crust intruded by arc magmatism. Backstripping of well data in the basin and margins suggested that Neogene extension was accompanied by crustal and lithospheric thinning [*Watts et al*., 1993]. Crustal thickness in the West Alboran Basin is poorly constrained but may exceed by far the thickness of ~15 km proposed for the Eastern Alboran Basin as deduced from seismic data

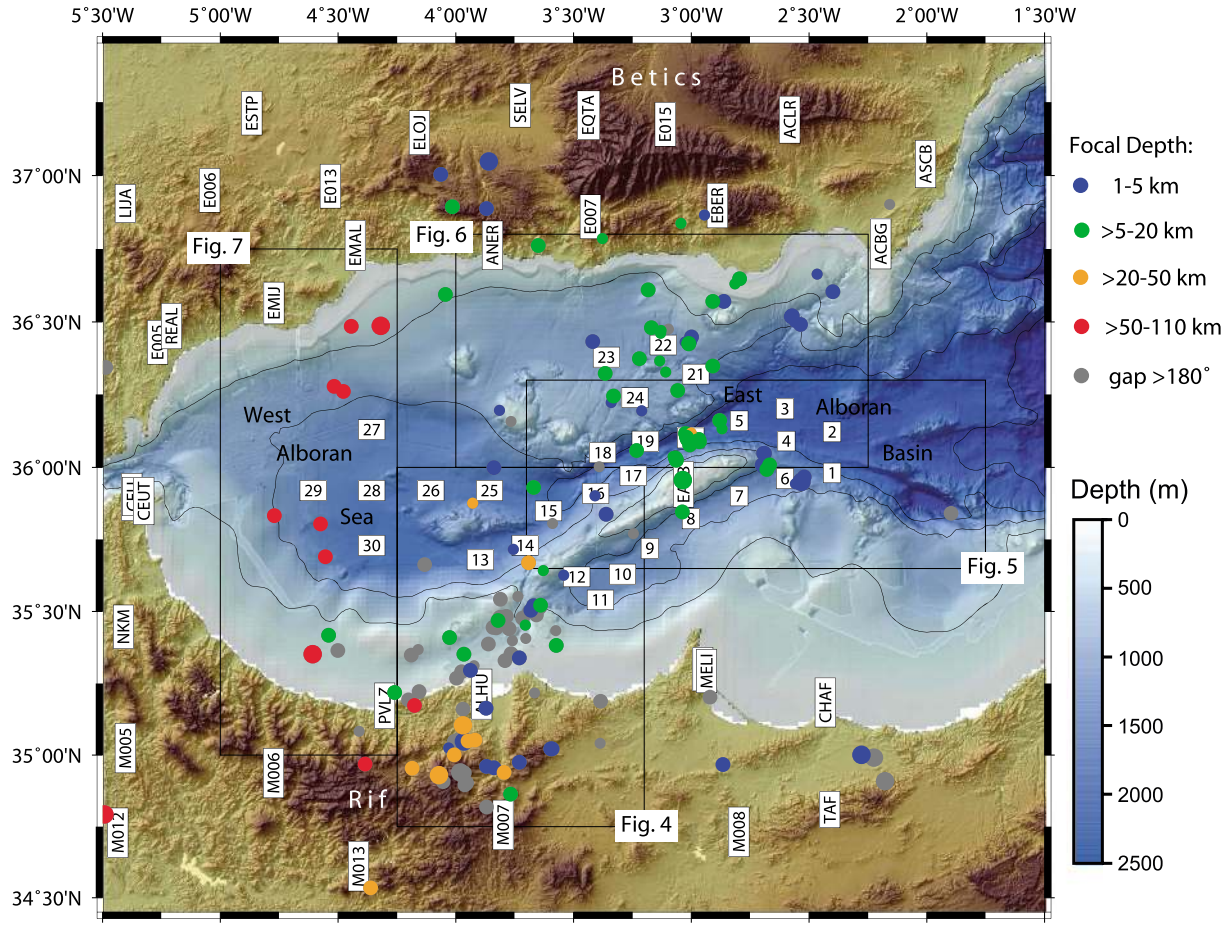

Figure 1. Amphibious seismological network in the Alboran domain. Regional topographic and bathymetric map of the southeast Iberian margin constructed from digital grids released by SRTM-3, IEO bathymetry [*Ballesteros et al.*, 2008; *Muñoz et al.*, 2008], BCSI-CSIC bathymetry [*Gràcia et al.*, 2006, 2012], and MEDIMAP [*MEDIMAP Group*, 2008] at 90 m grid size. Numbered squares are TOPO-MED ocean bottom seismometers (OBS), and labeled squares are TOPO-IBERIA land seismometers. Note that only land stations located in the vicinity of the coastline are shown. Colored dots are earthquakes coded by depth and quality. Grey dots are earthquakes with a gap >200°.

[*Booth-Rea et al.*, 2007]. Crustal thickness decreases eastwards, reaching ~6 km, and hence reflects oceanic crust flooring the Algero-Balearic Basin [*Booth-Rea et al.*, 2007].

Present-day tectonic stresses are controlled by the past subduction and the convergence between Africa and Europe, causing NW-SE shortening [*McClusky et al.*, 2003]. As a consequence, the Eastern Betic-Alboran Shear Zone [*Bousquet*, 1979] and the Trans-Alboran Shear Zone [*De Larouzière et al.*, 1988] formed, with rupture mechanisms indicating predominantly left-lateral strike-slip motion [*Stich et al.*, 2003a, 2006, 2010] with nearly N-S oriented *P* axes (~N170°E) and nearly E-W oriented *T* axes (~N80°E). In addition, some mechanisms include a minor component of normal faulting, consistent with the observed regional extension. In contrast, farther east in northern Algeria, reverse faulting with NW-SE (~N140°E) oriented *P* axes dominates [*Stich et al.*, 2003a]. Sub-bottom profiler and seismic reflection data clearly demonstrate this complex stress pattern, indicating diverse tectonic fabrics including extensional, compressional, and strike-slip structures [e.g., *Bourgois et al.*, 1992; *Watts et al.*, 1993; *Gràcia et al.*, 2006, 2012; *Martínez-García et al.*, 2011, 2013].

3. Seismological Data and Methodology

In the Alboran Sea, Betics, and Rif Cordilleras, two passive seismological experiments that overlapped in time nurtured each other. The first network covered the offshore domain, providing data from 30 German ocean bottom seismometers (OBS) in the western and eastern basins of the Alboran Sea. The deployment was part of the European Science Foundation (ESF) coordinated program TOPO-Europe. The second network complemented the offshore network, providing 155 temporary land stations in Spain, Morocco, and Portugal,

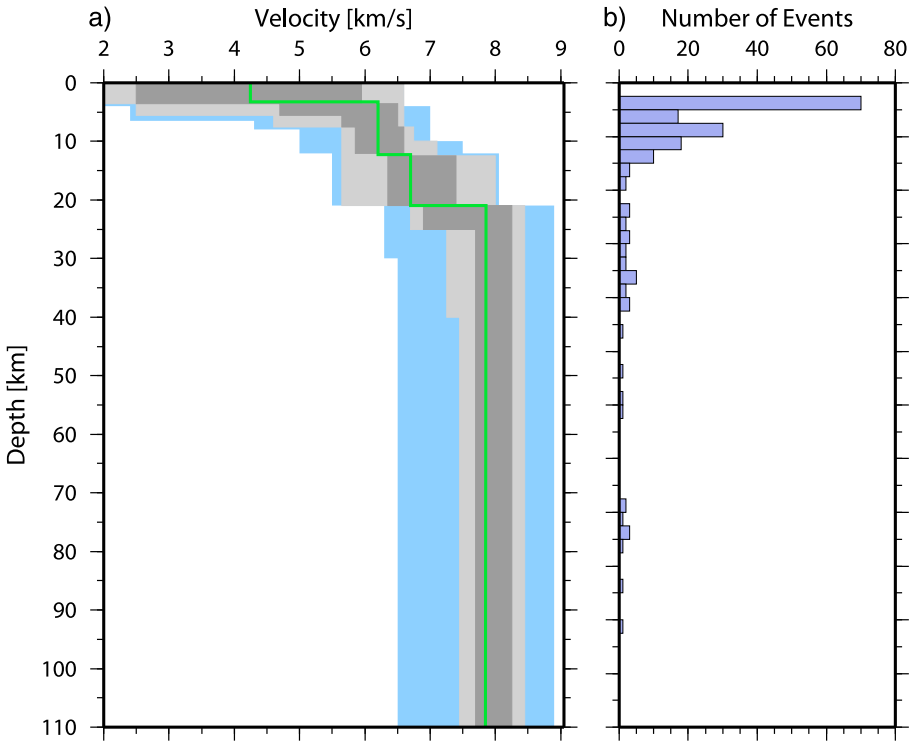

Figure 2. (a) Preferred minimum 1-D velocity model of the Alboran Sea (green line) computed by simultaneous inversion of arrival time data from local earthquakes for earthquake locations, seismic velocities, and station delays. Light blue area marks the range of starting models, light grey the range of all inversions, and dark grey the range of 75% of best inversion results. (b) Histogram of earthquake distribution as a function of depth.

being part of the Spanish TOPO-IBERIA project. Most earthquakes occurred in the Alboran Sea and were therefore well recorded by the marine network and the ~40 stations covering the coastal areas of Spain and Morocco (Figure 1), while stations farther in land just received the largest offshore events.

The offshore network was operated between 13 August 2009 and 15 January 2010. The network consisted of 30 OBS, including nine wide-band OBS operating a three-component Guralp CMG-40T (60 s) seismometer and a HighTech HTI-04-PCA/ULF hydrophone from the German DEPAS pool. In addition, 21 GEOMAR-OBS, equipped with a hydrophone and three-component short-period seismometers with a natural frequency of 4.5 Hz, were operated. To automatically detect seismic events in the continuous records a short-term-average versus a long-term-average (STA/LTA) trigger algorithm was applied to the OBS data. We used a STA window of 0.5 s and a LTA window of 60 s. The trigger parameters were applied to unfiltered vertical component data. We consider a trigger to be an earthquake when it was detected on four or more offshore stations. Applying these trigger parameters, visual inspection of the data suggest that we obtained generally less than ~10% false triggers and lose only those events that were recorded only on few stations, while all major events were included.

For event detection we extracted a 3 min long time window from the continuous OBS records and added the land stations, starting 20 s prior to trigger time. Events were registered in a SEISAN database [*Havskov and Ottemöller*, 2000], and *P* wave and *S* wave arrival times were handpicked. In total, we were able to locate 229 local earthquakes from the Alboran Sea. The reading weighting scheme ranges from factor 0, corresponding to the lowest uncertainty (±0.05 s), to factor 4 (>0.3 s) for doubtful readings that were not used. The total average *P* wave reading error is estimated at ±0.13 s.

For event location we calculated a minimum 1-D model (Figure 2) using the approach of *Kissling* [1988] and *Kissling et al.* [1994], and we located all earthquakes and explored the associated uncertainties using the nonlinear probabilistic location procedure NonLinLoc of *Lomax et al.* [2000]. For the inversion, the focal depth search has been limited to depth >1 km, avoiding in rare cases "water" quakes. Most earthquakes were

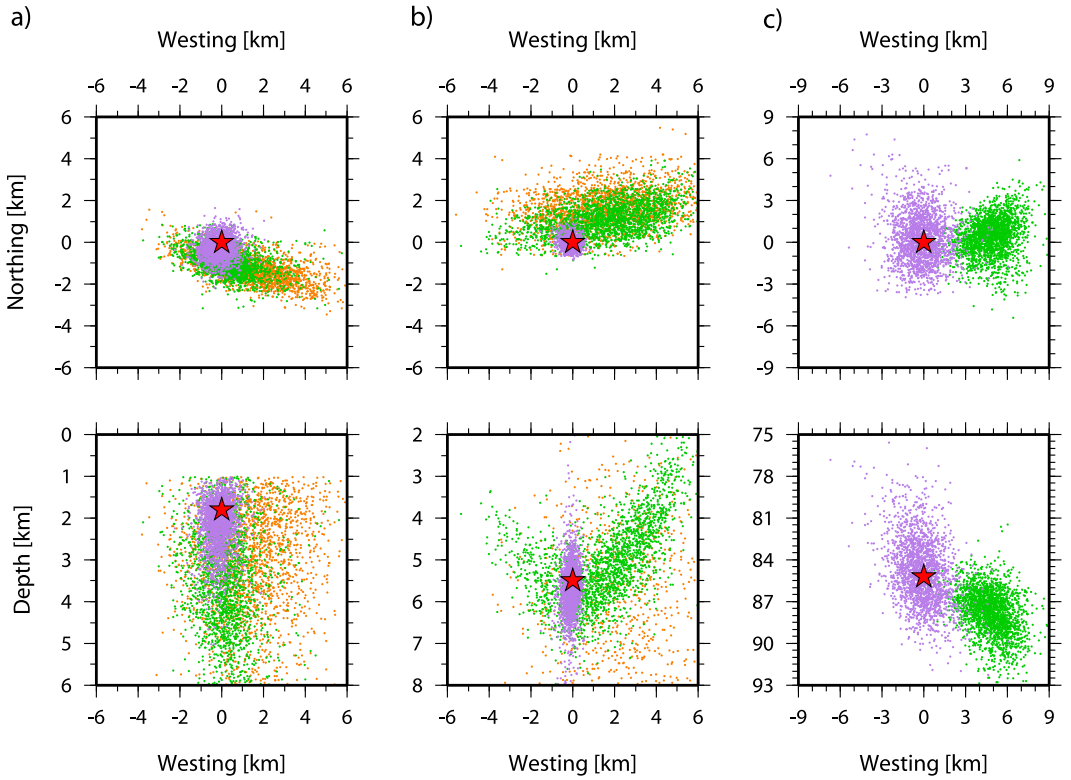

Figure 3. Plot of the probability density function (PDF) of three selected earthquakes (red stars). (a) Mw = 3.5 crustal earthquake below Alboran Island on 29th August 2009, (b) Mw = 3.4 crustal earthquake east of Alboran Ridge on 12th October 2009, and (c) Mw = 3.7 intermediate depth earthquake of 30th October 2009. Violet: probability density function (PDF) using all stations; light green: PDF without OBS; ochre: PDF without OBS and without station on Alboran Island.

crustal events with formal errors of ±0.5–2 km for the epicenter and ±1–1.5 km in focal depth. However, deeper earthquakes (>40 km) have larger epicentral errors of ±2–3 km and ±3–4 km in focal depth (Figure 3).

Further, we explored the benefit of an offshore network. We thus removed the OBS records from the catalogue and relocated the events. For most offshore events the uncertainty increased and errors roughly doubled (Figure 3). In addition, we removed the station on Alboran Island. The station clearly stabilizes the inversion and reduces uncertainties. For intermediate depth earthquakes in the West Alboran Basin, however, removal of the offshore stations had only a small impact on the estimated uncertainties, but locations were clearly biased by ~5 km toward the east and a few kilometers in depth (Figure 3c).

Moment magnitudes were estimated using the method of *Ottemöller and Havskov* [2003]. The two largest earthquakes were a Mw = 3.7 intermediate depth earthquake in the West Alboran Basin and a Mw = 3.5 crustal earthquake in the East Alboran Basin. Most events, however, had magnitudes of Mw = 1.5 to 2.8. The smallest earthquakes had magnitudes of Mw ~0.8 and were generally not included in the Instituto Geográfico National de Espana (IGN) catalogue.

First motion *P* wave polarities are commonly used to determine double-couple focal mechanisms of marine micro-earthquakes. Fault plane solutions were derived using the HASH and FOCMEC algorithms [*Hardebeck and Shearer*, 2002; *Snoke et al*., 1984]. We report mechanisms for a total of 14 earthquakes, for which both approaches provided similar solutions (Table 1).

4. Results

4.1. Minimum 1-D Model

The crustal structure of the Alboran Sea has been poorly surveyed using seismic techniques; thus, we have only limited information on its subsurface velocity structure. We therefore decided to derive a minimum 1-D model in order to obtain reliable hypocenter locations, particularly in focal depth. The minimum 1-D model

Table 1. Focal Mechanism From First Motion Polartites

Date	Time	Longitude	Latitude	Depth	Magnitude	Strike/Dip/Rake
20090829	0653	−2.536	35.949	1.8	3.5	240/67/68
20090903	1136	−2.909	36.571	8.9	2.9	221/67/46
20090908	0004	−7.825	36.000	50.0	3.8	232/41/−75
20090918	1722	−3.038	35.847	11.6	2.7	18/30/−178
20090920	1113	−2.277	35.002	3.9	3.2	160/75/−48
20090925	1637	−4.575	35.804	92.5	2.8	282/76/27
20091003	1351	−3.967	35.104	29.8	3.0	205/35/−30
20091006	1400	−2.965	36.089	12.7	2.8	127/73/58
20091012	1203	−3.034	35.956	5.6	3.4	103/44/22
20091012	1406	−3.009	36.42	11.6	2.8	66/38/−22
20091013	0935	−3.729	35.338	3.8	2.8	235/64/56
20091023	1302	−2.701	36.010	1.8	2.4	58/62/11
20091028	1721	−3.328	36.247	8.5	2.8	172/38/−47
20091030	0701	−4.310	36.499	85.2	3.7	295/73/71
20091112	0258	−3.062	36.025	8.5	2.1	58/34/−42
20091112	0325	−3.063	36.026	8.3	2.3	271/56/−53
20091209	0011	−4.541	35.702	100.9	3.0	66/71/−36

serves as an approximation for a full 3-D model and is suggested being close to the true earth model and includes station corrections that mitigate the effects of the structure close to the receiver and deviations from a simple laterally homogeneous model. The concept of the minimum 1-D model was introduced by *Kissling* [1988] and *Kissling et al.* [1994]. It is computed by simultaneous inversion of arrival time data from local earthquakes for hypocenter locations, seismic velocities, and station delays. Thus, the computation of a minimum 1-D model explicitly solves the coupled hypocenter-velocity problem.

The study area includes mountain belts like the Betics and Rif as well as offshore sedimentary basins that underlie the Alboran Sea. The total elevation differences between the deepest OBS2 at 1876 m below sea level and the highest station in the Betics EBER at 1690 m are on the order of 3.6 km (Figure 1), indicating large-scale topographic heterogeneities. Crust in the Alboran Sea is believed to comprise thinned continental crust, while the mountain belts will represent thickened crust [*Banda et al*., 1993; *Watts et al*., 1993; *Booth-Rea et al*., 2007]. Thus, a minimum 1-D model can only be a crude approximation for the entire region. However, in our approach we concentrate on earthquakes that triggered the OBS network, and thus, their sources occur preferentially in the Alboran Sea region. Therefore, the 1-D velocity model will basically approximate the offshore structure. Thus, major changes in topography and crustal thickness will therefore be condensed into the station delays (corrections) for the land stations.

We first established a number of starting models, searching for robust features. The topmost layer, however, would correspond to a thick sedimentary unit imaged in seismic reflection data [e.g., *Comas et al*., 1995; *Booth-Rea et al*., 2007] with velocities of ~3 km/s to 5 km/s. Crustal thickness in the East Alboran Basin is of the order of 15 km [*Booth-Rea et al*., 2007] but might be thicker in the West Alboran basin, reaching 35 km in the Betics [*Banda et al*., 1993]. In addition to our suite of starting models, we considered the velocity models used by *Stich et al*. [2003a] for regional moment tensor waveform inversion. *Stich et al*. [2003a] used three different 1-D models, reflecting differences in crustal structure for the Alboran Sea (model A), mountain belts (model B), and continental domains such as the Iberian mainland (model C).

Initially, we located all earthquakes using the model A of *Stich et al*. [2003a]. For computation of the reference model, we restricted the data set to earthquakes that were observed at least at six stations, with a gap $< 180°$, and occurring at 2 km depth or deeper. Of the 229 earthquakes, just 61 fulfill these criteria. This is due to the fact that we restricted our analysis to earthquakes that triggered the offshore network. Earthquakes that did not fulfill these criteria were excluded. In consequence, earthquakes included in the computation of the minimum 1-D model occurred predominately in the Alboran Sea and in the coastal areas of Spain and Morocco. Of course, within the entire TOPO-IBERIA network the total number of detected earthquakes was much larger.

First, we inverted for the *P* wave velocity structure (Figure 2). We tested a number of different models with variable discretization in depth. However, with respect to the quality of the misfit as expressed by the root

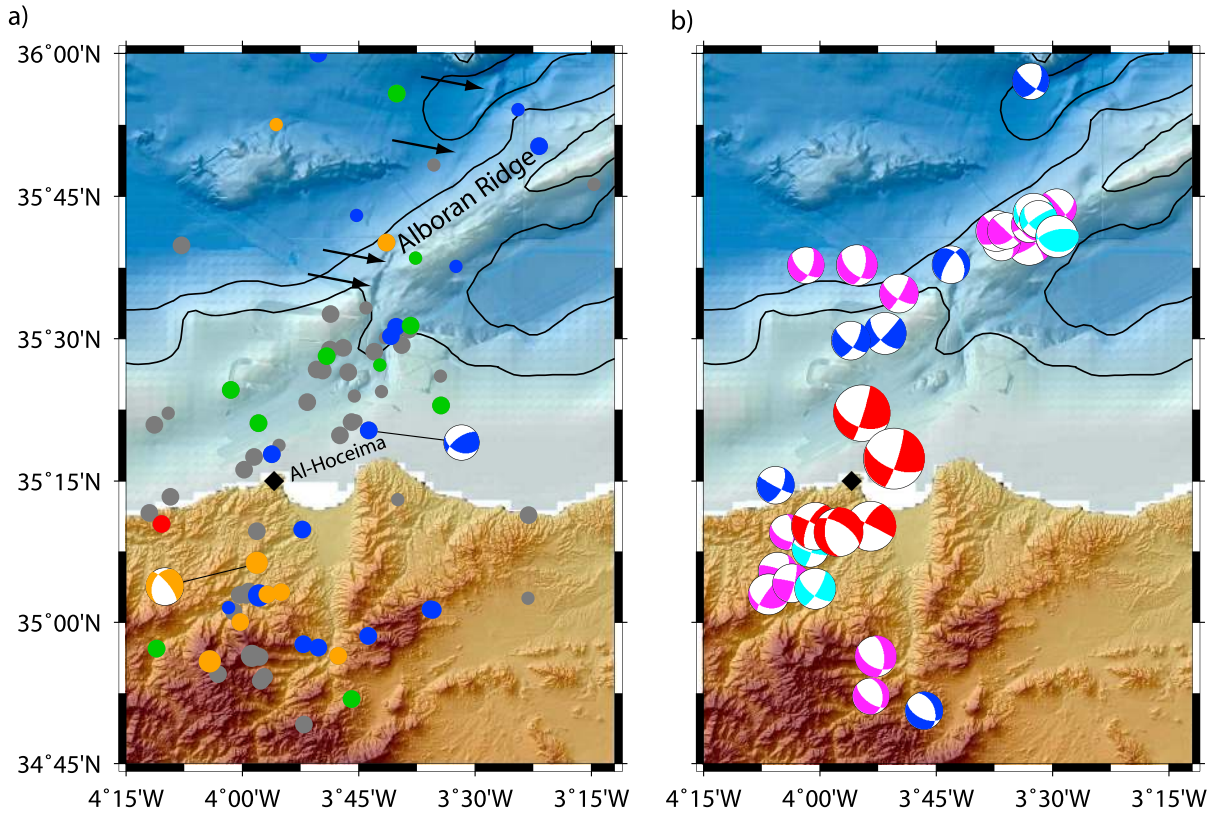

Figure 4. (a) Distribution of seismicity and first motion focal mechanisms at the Moroccan margin, color coding as in Figure 1. (b) Same area with focal mechanisms from moment tensor inversion. In red, gCMT (http://www.globalcmt.org/CMTsearch.html); in other colors, mechanisms from *Stich et al.* [2003a, 2005, 2006, 2010]. Mechanisms are scaled by magnitude; arrows indicate fault traces.

mean square (RMS) error between observed and calculated travel times, models with a larger number of layers in depth did not show better results. We thus chose for most models discontinuities around 3.5, 12, 21, 25, and 120 km. In the upper crust, however, the earthquake data provide few constraints on uppermost velocity structure and the resolution is poor. Different starting models with velocities of 3 to 6 km/s provide reasonably similar estimates. The velocity of this layer is therefore set to 4.25 km/s, which is the resulting velocity of an inversion with the model A of *Stich et al.* [2003a] and is close to the majority of inversion outputs. We thus fix the velocity in the uppermost sedimentary layer to 4.25 km/s. The second layer extends to a depth of ~12 km. After inversion, velocities of 5.6 to 6.6 km/s provide a reasonable fit, with more than 75% of the models being in the range of 5.85 to 6.5 km/s. Down to a depth of ~21 km, velocities range from 5.6 to 8 km/s, with more than 75% of inversion results ranging from 6.35 to 7.4 km/s. Between 20 and 120 km depth, most inversion results range from 7.7 to 8.25 km/s. The best solutions provide an average RMS misfit of ~0.35 s and may suffer from the large structural heterogeneity of the Alboran, Betics, and Rif domain. The model A caused a misfit in the order of the best fitting velocity model and hence provided a reasonable approximation of the *P* wave velocity structure. The models B and C yield average RMS misfits of 0.447 s and 0.432 s, respectively.

We note that the location procedure of LonLinLoc iteratively updates station corrections and hence minimizes the misfit. The final overall average RMS misfit for the 229 located events is 0.28 s, with misfit values ranging from 0.04 s to 0.69 s. Later, *S* wave arrivals were included in the inversion, and a *S* wave velocity model was derived. For the *S* wave velocity inversion, *P* wave velocity was damped and basically kept constant. The best fit average Vp/Vs ratio is 1.75, with estimates ranging from 1.8 to 1.65.

4.2. Seismicity

Crustal seismicity in the Alboran Sea is most prominent along a NE-SW trending zone, roughly linking the Spanish coast near the city of Adra with the Moroccan coast near the city of Al Hoceima, The seismicity zone is roughly 20 to 40 km wide (Figures 1 and 4–7). The level of activity, however, varies significantly both in space and time.

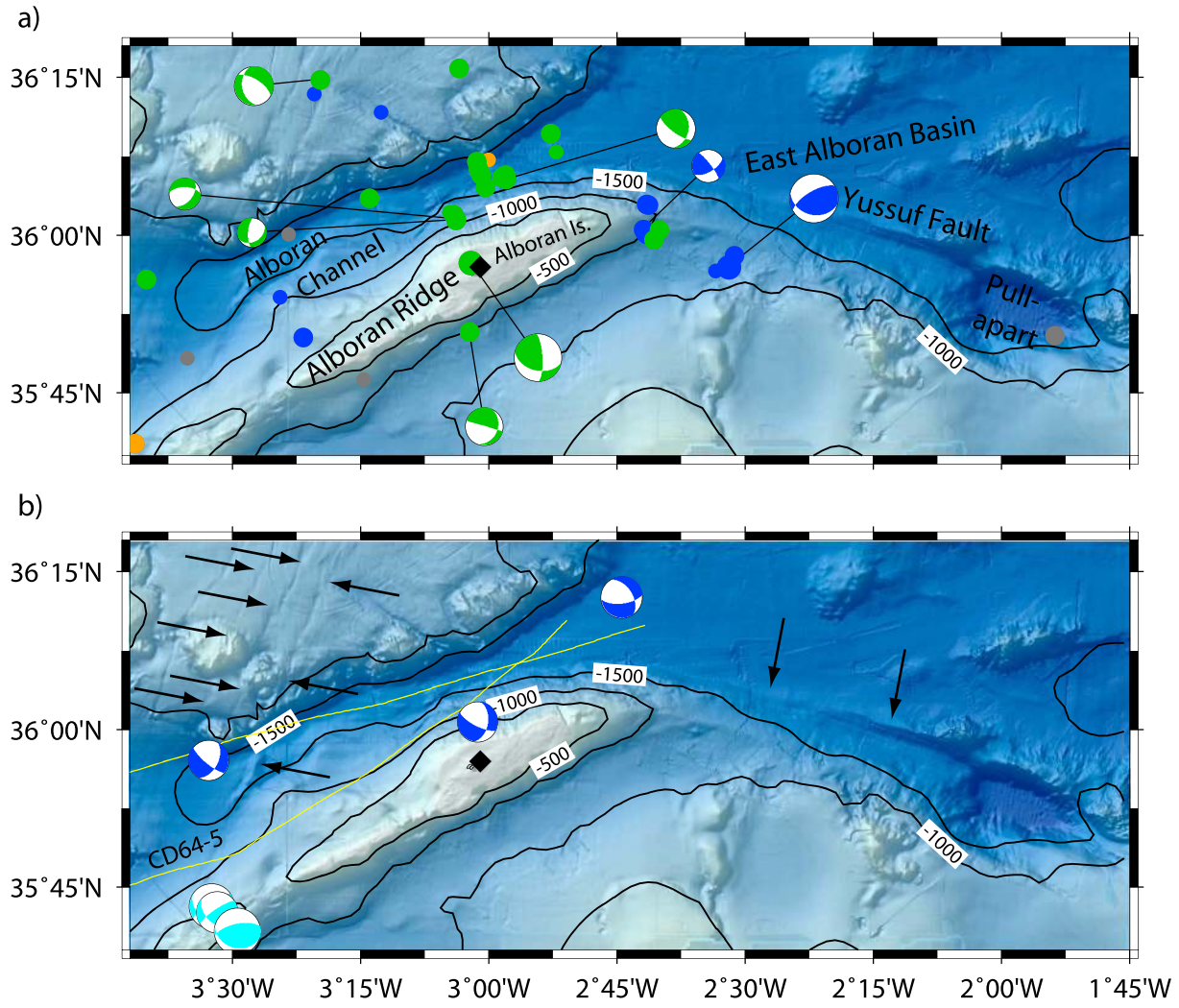

Figure 5. (a) Distribution of seismicity and first motion focal mechanisms in the vicinity of the Alboran Ridge, color coding as in Figure 1. (b) Same area with focal mechanisms from moment tensor inversion [*Stich et al.*, 2003a, 2006, 2010]; mechanisms are scaled by magnitude; yellow line indicate seismic reflection profile from cruise CD64; arrows indicate fault traces.

4.2.1. Northern Morocco—Al Hoceima

Seismicity was not evenly distributed within the survey area but is clustered with most earthquakes occurring in Morocco to the south of the city of Al Hoceima and between Al Hoceima and the southern tip of the Alboran Ridge (Figures 1 and 4), an area that was hit by large strike-slip earthquakes in 1994 (Mw = 5.9) [*Calvert et al.*, 1997; *Akoglu et al.*, 2006] and in 2004 (Mw = 6.3) [*Stich et al.*, 2005]. All earthquakes occurred outside of the marine network that was used for triggering and hence emphasized that this area was seismically the most active region during the offshore deployment. Unfortunately, stations in Morocco often had a poor signal to noise ratio. Thus, a large number of events recorded in the vicinity of Al Hoceima had a large azimuthal gap, and thus, trade-offs between focal depth and epicentral location caused large uncertainties. However, most earthquakes in this domain tended to occur at crustal levels, with some occurring at 30–35 km depth. Due to the fact that the 1-D seismic velocity model may be associated with the thinner crust of the offshore domain, some of the deeper earthquakes are perhaps affected by a biased velocity model. However, seismicity in the coastal domain of Morocco tends to occur at greater depth than most events located in the central Alboran Sea.

4.2.2. The Alboran Ridge

The Alboran Ridge is a constructional volcanic ridge of Pliocene age and is the most prominent feature of the entire basin (Figures 1 and 5). However, during the deployment along the ridge, only a small number of earthquakes occurred. Reliable focal mechanisms could be obtained for seven events. To the south of

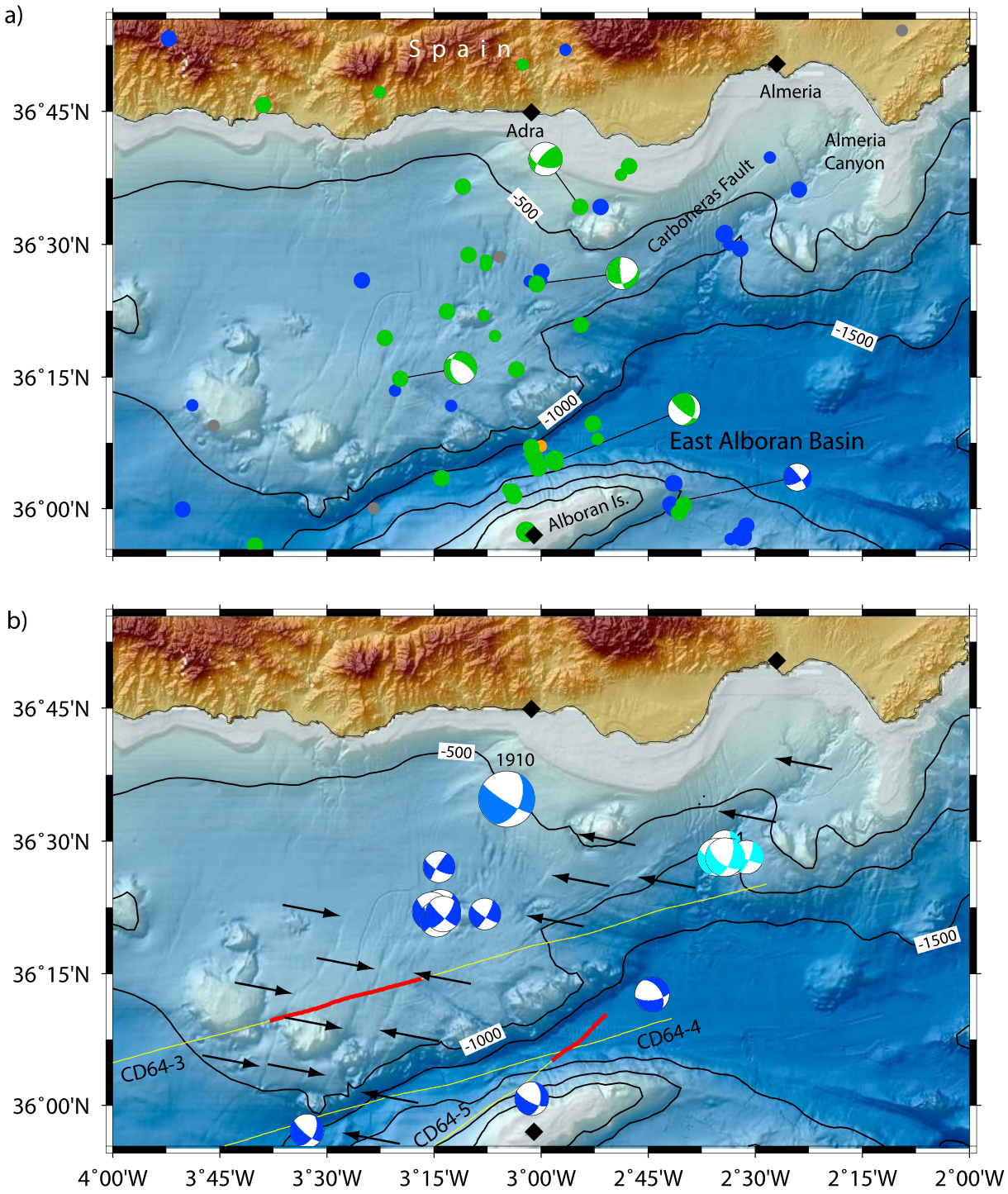

Figure 6. (a) Distribution of seismicity and first motion focal mechanisms off the Spanish coast, color coding as in Figure 1. (b) Same area with focal mechanisms from moment tensor inversion [*Stich et al.*, 2003a, 2006, 2010]. Also shown is the mechanism for the Mw = 6.1 1910 Adra earthquake [*Stich et al.*, 2003b]; mechanisms are scaled by magnitude. Yellow line indicates seismic reflection profile from cruise CD64. Thick red lines indicate data shown in Figure 8; arrows indicate fault traces.

Alboran Island, two well-located earthquakes occurred, showing normal to strike-slip motions. One of them was the largest crustal earthquake recorded in the Alboran Sea: the Mw = 3.5 earthquake of 29th August 2009. To the NW of Alboran Island, two events occurred, indicating extensional mechanisms. Further, a small sequence of nine earthquakes occurred to the NE of Alboran Island, beneath the Alboran Channel at the western edge of the East Alboran Basin. Seismic reflection data acquired by the RRS Charles Darwin along profiles CD64-4 and CD64-5

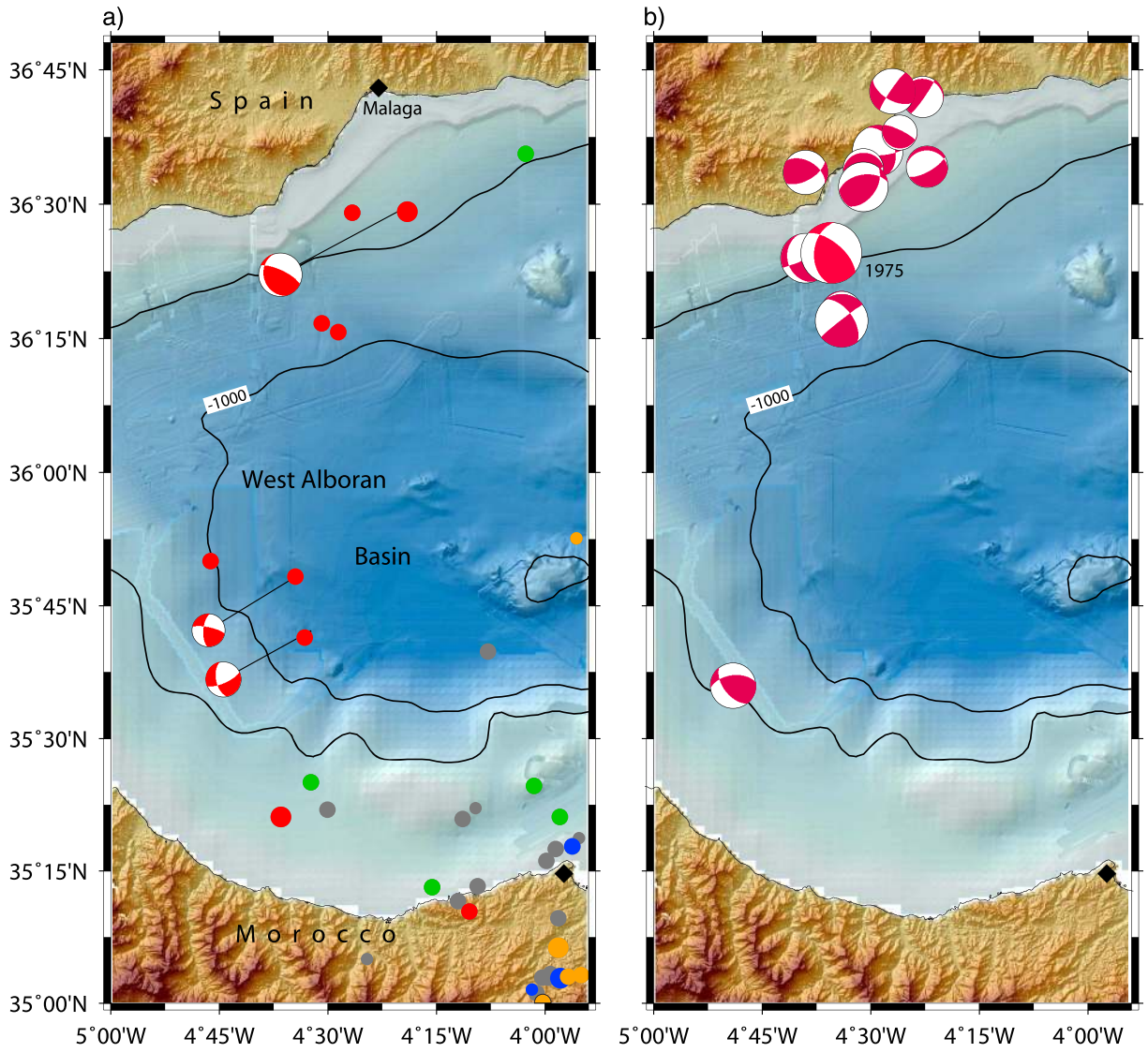

Figure 7. (a) Distribution of seismicity and first motion focal mechanisms for the seismicity in the West Alboran Basin, color coding as in Figure 1. (b) Same area with focal mechanisms from *Buforn et al.* [2004]; light red mechanisms indicate $M = 5.2$ earthquake of 7th August 1975; mechanisms are scaled by magnitude.

across this area imaged a number of NW-SE trending faults (Figure 8), many of which offset the seafloor. One earthquake on 6th October 2009 provided a focal mechanism similar to those occurring near Alboran Island and hence indicating oblique normal faulting. Note, all events occurring in the vicinity of Alboran Island indicated roughly southeastward trending *T* axes. However, overall stress patterns are rather heterogeneous.

At the easternmost tip of Alboran Ridge, near the escarpment facing the East Alboran Basin, a sequence of earthquakes occurred (Figure 5a). One earthquake indicated strike-slip motion with a north facing *P* axis and southeast facing *T* axis. Roughly 10 km farther east, the second largest event recorded in the Eastern Alboran Basin occurred. It was a Mw = 3.4 earthquake rupturing on 12th October 2009. Its focal mechanism indicates thrusting; the *P* axis trends northwestward to northward, roughly mimicking the northwest-southeast oriented compression in agreement with plate convergence.

The northern termination of the Alboran Ridge seems to be tectonically linked to the east with the Yusuf pull-apart basin (Figure 5) and Algerian margin [e.g., *Martínez-García et al.*, 2013]. The structure linking these features, the right-lateral Yusuf Fault, is generally interpreted as the lithospheric boundary between the African and Eurasian plates in the Eastern Alboran Sea. However, during the time of network operation the Yusuf Fault remained seismically quiet and only a small number of events occurred to the south of the fault

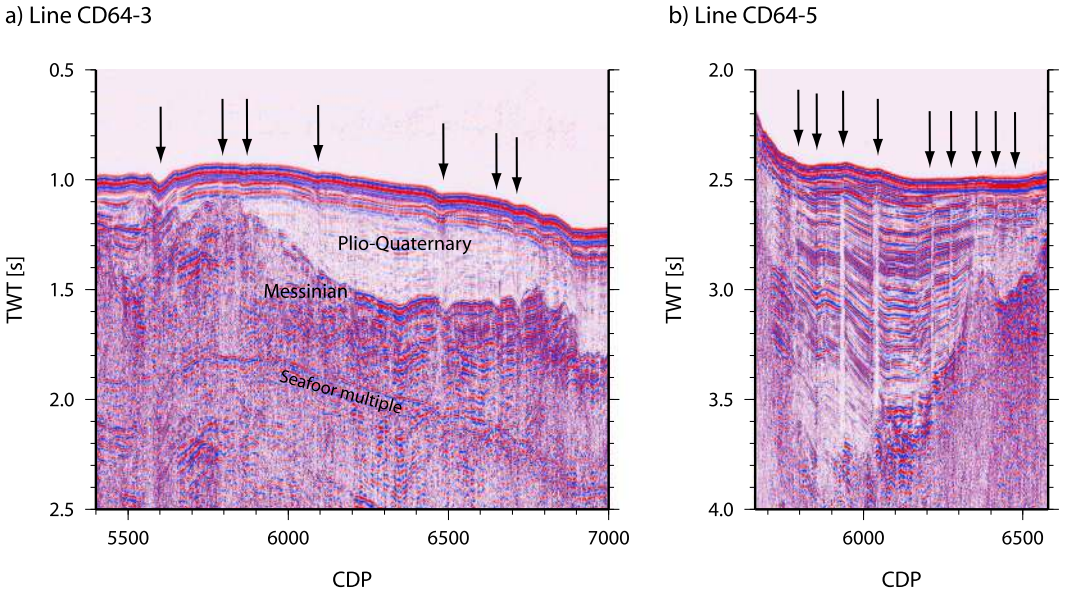

Figure 8. Seismic reflection data from the RRS *Charles Darwin* cruise CD64 (for location, see Figure 6). (a) Profile CD64-3 across the Adra anticline region; (b) profile CD64-5 across the easternmost East Alboran Basin. Arrows mark near vertical faults.

trace. Stress patterns were variable, indicating both strike-slip motion and compression. At the Yusuf basin, only a single earthquake was detected. However, as the pull-apart basin was outside of the OBS network, our capacity to detect earthquakes in the region was limited.

Earthquakes in the central Alboran Sea and those offshore SE Spain generally occurred at much shallower depth than those in the vicinity of Al Hoceima in northern Morocco. Earthquakes generally occurred above 15 km and most events ruptured between 10 and 2 km depth.

4.2.3. The Adra-Almeria Margin

The SE Spanish Margin hosts one of the largest strike-slip faults of the Alboran Sea, the left-lateral Carboneras Fault (Figures 1 and 6). The surface morphology of the offshore segments of the fault has been imaged in bathymetric, sub-bottom profiler, and side-scan sonar data [*Gràcia et al.*, 2006]. Deflection of channels and gullies, pressure ridges, and flower structures are observed along the more than 100 km long fault trace (Figure 6). During our campaign, the fault was seismically relatively inactive, although two earthquakes occurred along the fault. Interestingly, most earthquakes in the Gulf of Almeria occurred along the Almeria Canyon, perhaps suggesting that the canyon is controlled by a fault at depth.

Most events off the coastline of SE Spain occurred to the south and the SW of the town of Adra. In the area, bathymetric data show a large number of NE-SW trending features (Figure 6b), which have been suggested being faults [e.g., *Ballesteros et al.*, 2008; *Martínez-García et al.*, 2011; *Gràcia et al.*, 2012]. Most epicenters seem to align along these structures. Only three earthquakes provided fault plane solutions, indicating oblique normal or strike-slip faulting.

4.2.4. The West Alboran Basin

In the West Alboran Basin the level of seismicity was much lower than along the Trans-Alboran Shear Zone. Furthermore, shallow crustal earthquakes are very sparse. The majority of events occurred at a depth range of 60 to 100 km, including the largest earthquake recorded during the offshore deployment: the Mw = 3.7 event of 30th October 2009 to the south of Malaga at 85 km depth. These intermediate depth events occurred in a narrow band between the coast of Morocco and Spain. Three earthquakes provided focal mechanisms, indicating oblique dip slip or thrust motion and had similar stress pattern.

5. Discussion

5.1. Seismic Structure of the Alboran Sea

The Alboran Sea is a rifted basin that developed in the Early Neogene. Backstripping of well data suggested that the basin was affected by subsidence and hence a major rifting episode about 20 Myr ago, indicating

rapid tectonic subsidence between 22 to 16 Myr ago and a slower thermal subsidence being related to lithospheric thinning [*Watts et al*., 1993]. Gravity modeling suggested that the crust has been thinned by a factor of ~1.7 from about ~30–36 km beneath the Rif and Betic orogenic belts to ~20 km beneath the Alboran Sea basin, consistent with tectonic subsidence analysis of deep commercial wells [*Watts et al*., 1993]. The minimum 1-D model derived from the joint inversion of earthquake arrival times for hypocentral parameters and velocity structures indicates an average crustal thickness of ~21 km (Figure 2). Thus, crust seems to be thicker than in the East Alboran Basin, where crust is in the order of 15 km [*Booth-Rea et al*., 2007], but thinner than the crust of the adjacent Betics, which is in the order of 35 km [*Banda et al*., 1993]. Consequently, the reference velocity model supports the interpretation that the Alboran Sea is floored by thinned crust, most likely of continental origin.

Seismic velocities derived from the inversion procedure indicates upper and lower crustal velocities of ~6.2 km/s and ~6.6 km/s, respectively. Crustal velocities of $<$7 km/s are supported by local earthquake tomography for the Alboran domain [*El Moudnib et al*., 2015]. Thus, velocities range indeed within the values expected for continental crust [*Christensen and Mooney*, 1995] rather than indicating typical arc-like crust with seismic velocities of the lower crust of 7 km/s or faster [e.g., *Contreras-Reyes et al*., 2011]. Consequently, both the velocity-depth structure and crustal thickness support the interpretation that the Alboran Sea represents extended continental crust, as envisioned by *Watts et al*. [1993] and *Comas et al*. [1999]. In addition, ODP Leg 161 sampled the basement in the West Alboran Basin, indicating the presence of metamorphic rocks of continental origin [e.g., *Comas et al*., 1999]. However, the occurrence of calc-alkaline to alkaline arc-type rocks drilled and dredged from volcanic outcrops in the Alboran Sea suggests that continental crust has been intruded by arc magmas in the Miocene [*Duggen et al*., 2003, 2004].

5.2. Linking Seismic Activity With Alboran Basin Faults

5.2.1. The Northern Moroccan Margin

The area around the city of Al Hoceima on the northern Moroccan Mediterranean coast experienced a major Mw = 6.3 earthquake on the night of 24 February 2004, which caused 628 casualties and more than 2500 buildings collapsed [*Stich et al*., 2005]. *Stich et al*. [2005] placed the epicenter about 10 km to the south of Al Hoceima near the village of Ait Kamra. Earlier, on 26th May 1994 the same area experienced a Mw = 5.9 earthquake with a centroid seaward of the Al Hoceima event. The 1994 and 2004 earthquakes and most aftershocks indicated predominately left-lateral strike-slip faulting with most earthquakes occurring between 10 and 15 km depth [*Stich et al*., 2005]. However, a few aftershocks had a clear normal transtensive component, similar to the mechanism observed during our field work.

The area of intense seismic activity observed during our deployment roughly coincides with the area affected by the 2004 Mw = 6.3 Al Hoceima earthquake and its aftershocks, suggesting that even 5 years after this major earthquake postseismic stress pattern controls seismicity. Alternatively, new stresses may build up. The majority of aftershocks occurred above 20 km [*Stich et al*., 2005]. Similar patterns were observed previously by *Calvert et al*. [1997], monitoring the aftershocks of the Mw = 5.9 1994 earthquake, indicating that most aftershocks occurred at depth of $<$15–20 km. Thus, it is striking that aftershocks occurred generally at a shallower level than some of our events of the Al Hoceima sequence, occurring at 30 to 35 km. Some of the Moroccan stations had a rather poor signal to noise ratio. Thus, in the location procedure those picks had a lower weight than the higher quality data on the OBS stations. We therefore cannot rule out trade-offs between focal depth and epicenter and hence large uncertainties of focal depth.

At the southwestern end of the Alboran Ridge, sub-bottom profiler data depicted a narrow NNE-SSW trending zone with folding and reverse faulting [*Martínez-García et al*., 2011]. This zone of deformation may define a seismogenic, left-lateral strike-slip fault zone that seems to be connected to the south with the Al Hoceima seismic swarm [e.g., *d'Acremont et al*., 2014] and belongs to the Al Idrisi Fault Zone introduced by *Martínez-García et al*. [2011]. Stress patterns from regional moment tensor inversion (Figure 4b) of Mw ~3.5 to 4.8 earthquakes [*Stich et al*., 2003a, 2006, 2010] indicated that strike-slip faulting is the most prominent fault type approaching the southern tip of the Alboran Ridge, where the fault may splay. One fault zone may run roughly parallel to the Alboran Ridge, while the other fault system, the Al Idrisi Fault Zone, may connect the southern Alboran Ridge with faults imaged in the bathymetry to the southwest of Adra and Almeria [*Ballesteros et al*., 2008; *Martínez-García et al*., 2011, 2013]. The second branch can readily be seen in the bathymetry, but it remained seismically quiet during our monitoring

efforts. *Martínez-García et al*. [2013] proposed that the Al Idrisi Fault Zone system north of Al Hoceima initiated at the end of the Late Pliocene and is active since 2 Myr ago.

The style of faulting at the southern Alboran Ridge deduced from seismic reflection data reflects complex stress pattern, including southwest-northeast oriented trusting as indicated by folding [e.g., *Bourgois et al*., 1992; *Mauffret et al*., 2004, 2007; *Martínez-García et al*., 2013].

5.2.2. The Alboran Ridge

The Alboran Ridge, with a length of ~130 km, is the most prominent feature in the Alboran Basin (Figures 1 and 5) and rises from ~1800 m to above sea level at Alboran Island, a small 15 m high platform. The Alboran Ridge has been formed by Neogene to Quaternary volcanic activity [*Comas et al*., 1999; *Booth-Rea et al*., 2007] that was related to back-arc extension and arc-like magmatism [*Duggen et al*., 2004]. Today, the convergence between Africa and Eurasia controls the tectonics of the Alboran domain. The ridge indicates recent uplifting and deformation that has been caused by subvertical, strike-slip, and reverse faults with associated folding in the shallower sediments [*Martínez-García et al*., 2013]. Further, the opposite vergence of thrust faults bounding the base of the ridge supports compressional tectonics [e.g., *Bourgois et al*., 1992]. Seismicity is sparse in the area and neither seismicity nor stress pattern from focal mechanisms supports any clear fault system, indicating that stresses and hence faulting vary both temporary and spatially. Such a scenario is supported by seismic reflection data, which show that deformation is distributed over a broader area and that both compressional [*Bourgois et al*., 1992; *Martínez-García et al*., 2011] and strike-slip styles of faulting [*Martínez-García et al*., 2011] characterize the region.

In the central Alboran Sea, most micro-earthquakes occurred at the western edge of the East Alboran Sea where the Alboran Channel opens into the eastern basin. Bathymetric data did not indicate any clear fault pattern; however, legacy multichannel seismic reflection data indicate the presence of NW-SE trending faults across the Alboran Channel [e.g., *Watts et al*., 1993; *Martínez-García et al*., 2013], including faults imaged along RRS Charles Darwin profiles CD64-4 and CD64-5 (Figure 8b). These subvertical faults offset the seafloor and may have an important strike-slip component, although the stratigraphy indicates shortening at the northern end of the Alboran Ridge, as suggested by *Martínez-García et al*. [2013]. The tectonic fabric of the seismic reflection data hence mimics the stress pattern observed in a single focal mechanism for the earthquake cluster.

5.2.3. The Almeria-Adra Margin

The most prominent fault in the Gulf of Almeria is the 100 km long NE-SW trending left-lateral strike-slip Carboneras Fault [*Gràcia et al*., 2006], which also runs onshore for more than 50 km as part of the southern termination of the Eastern Betic Shear Zone [*Bousquet*, 1979], the most seismically active area in Spain (Figure 6). Numerous earthquakes that affected the city of Almeria in historical times, such as years 1487, 1522 (IX MSK), 1658 (VIII MSK), and 1804 (IX MSK), were attributed to motion along the Carboneras Fault [*Keller et al*., 1995; *Reicherter and Hübscher*, 2007]. Detailed bathymetry, side-scan sonar mosaics, and high-resolution sub-bottom profiles across the Carboneras Fault showed upward-splaying subvertical faults, defining positive flower structures [*Gràcia et al*., 2006]. Geomorphic features typically found in subaerial strike-slip faults, such as deflected drainage, shutter ridges, pressure ridges, and en echelon folds (Figure 6), suggested a strike-slip motion combined with a vertical component along the submarine trace of the fault [*Gràcia et al*., 2006]. Seismically, however, only a very small number of events might be associated with the Carboneras Fault (Figure 6a), suggesting that the fault is quiet, either temporarily inactive, or creeping, or locked. In the Gulf of Almeria, however, a number of earthquakes occurred along the Almeria canyon and channel system, where moment tensor inversion found strike-slip motion (Figure 6b), associated with NNE-SSW left-lateral or WNW-ESE trending fault zones [*Stich et al*., 2010].

Earthquakes to the southwest of the town of Adra seem to be related to elongated features in the bathymetry; *Ballesteros et al*. [2008] interpreted them as either cracks or faults. High-resolution sub-bottom profiler data suggested that these features might correspond to faults [*Martínez-García et al*., 2011, 2013]. Seismic reflection profile CD64-3 (Figure 8a) shows that the elongated features are indeed corresponding to active deeply penetrating faults. Although events cannot be attributed to a particular fault, the recorded earthquakes demonstrate the seismically active nature of this fault region. A number of moment tensor estimates for earthquakes occurring in the vicinity of these faults (Figure 6b) support strike-slip motion [*Stich et al*., 2003a]. These mechanisms roughly approximate the focal solution of the 1910 Mw = 6.1 (MSK ~ VI) Adra earthquake [*Stich et al*., 2003b]. It thus might be reasonable to hypothesize that these events share a common origin. However, one of our focal mechanisms suggests that the northeast-southwest trending faults also have an extensional component. Furthermore, on the basis of swath bathymetry data and high-resolution seismic reflection Sparker profiles offshore Adra,

Gràcia et al. [2012] suggested that the 1910 Adra earthquake may have occurred along the 20 km long, NW-SE trending Adra Fault with a normal-dextral component. This suggests that additional data are needed to nurture our understanding of active fault systems in the area and reveal potential future hazards associated with those features.

The interpretation of a NE-SW trending seismicity band connecting the Al Hoceima sequence with the seismicity offshore Adra and Almeria margins supports the concept of a Trans-Alboran Shear Zone, as initially defined by *De Larouzière et al*. [1988], although not as a single, unique large structure as some authors have later proposed [e.g., *Gutscher*, 2004]. The Trans-Alboran Shear Zone is also supported by GPS measurements, assessing motion and active deformation along the African-Eurasian plate boundary [*Koulali et al*., 2011]. Based on seismic data and biostratigraphic data from wells, *Martínez-García et al*. [2013] proposed that the Al Idrissi Fault to north of Al Hoceima is part of a larger fault system that coincides with the NE-SW trending corridor of shallow crustal seismicity across the Alboran Sea (Figure 1).

Structurally, the Trans-Alboran Shear Zone is associated with faster *P* wave velocity than rocks to the west and east, most clearly between 8 and 24 km depth [*El Moudnib et al*., 2015]. *El Moudnib et al*. [2015] suggested that the higher velocities may correspond to a mechanically stronger block stretching across the Alboran Sea and may coincide with rocks of an immature volcanic arc or magmatic intrusions associated with Miocene arc volcanism [*Duggen et al*., 2003].

5.2.4. The West Alboran Basin

Seismicity in the West Alboran Basin occurs at much deeper levels than in the East Alboran Basin and hence is not associated with any surface expression of faulting (Figure 7a). Seismicity recorded with our network occurred in a narrow 20 to 30 km wide band of intermediate depth seismicity at 60 to 110 km, in agreement with the seismicity pattern previously obtained from regional networks [e.g., *Buforn et al*., 2004]. It also coincides with faster seismic velocities indicating the occurrence of a subducted slab with one or more tears [e.g., *Sparkman and Wortel*, 2004; *García-Castellanos and Villaseñor*, 2011; *Pedrera et al*., 2011; *Ruiz-Constán et al*., 2011]. If still moving westward or sinking, the slab may affect regional stresses and hence may cause some extension in the back arc [*Heuret and Lallemand*, 2005] and hence eastern Alboran Sea. However, geodynamic modeling suggests that the slab is stalled since 8 Ma [*Chertova et al*., 2014]. Consequently, subduction may have little impact on the regional stress field.

The stress pattern derived for intermediate depth earthquakes showed rather variable features [e.g., *Buforn et al*., 2004; *Ruiz-Constán et al*., 2011]. However, most mechanisms indicated predominately vertical motion. Our mechanisms generally support this pattern with a similar fault motion for the three events with focal mechanisms (Figure 7b). The largest event recorded during the amphibious network operation was the Mw = 3.7 earthquake of 30th October 2009 occurring at 85 km depth. It occurred in the vicinity of the $M = 5.2$ event of 7th August 1975 and had a nearly identical mechanism [*Buforn et al*., 2004]. However, the complex structure of the area with large changes in crustal thickness and topography may affect fault plane solutions derived from first motions. Thus, take-off angles might be biased and hence may cause inconsistent fault plane solutions or may not allow proper separation of polarity readings into quadrants.

5.3. Depth Distribution of Seismicity, Thermal Considerations, and Seismic Hazard Potential

Earthquakes in the offshore Alboran domain occurs predominately at a depth $<$10–15 km. Deeper seismicity is only observed in the western basin, where earthquakes occurred at 60 to 110 km depth. Further, approaching the southern margin of the Alboran Sea, some earthquakes tend to occur at 20 to 40 km and hence at greater depths.

In the Imperial Valley and Peninsular Ranges of California (USA), *Doser and Kanamori* [1986] found that crustal heat flow and focal depths are correlated. In the Peninsular Ranges the majority of earthquakes occurred at greater depth than in Imperial Valley where the heat flow is nearly double that of the Peninsular Ranges. A similar correlation was found in northeast Japan, indicating that focal depth peaks at shallower depth when heat flow is increased [*Tanaka and Ishikawa*, 2002].

In Iberia and across the Gibraltar Arc, heat flow varies considerably. Iberia has a crustal heat flow of 60 to 80 mW/m^2 [*Fernàndez et al*., 1998]. The lowest values of 40 to 50 mW/m^2 are observed in the Gulf of Cadiz, west of the Strait of Gibraltar [*Grevemeyer et al*., 2009], whereas the highest values occur in the East Alboran Basin with a crustal heat flow of $>$120 mW/m^2 [*Polyak et al*., 1996].

We approximate the temperature T within the crust as a function of depth z using a simple geotherm. Thus,

$$T(z) = -[A/2\,k]\,z^2 + [Q_0/k]\,z + T_0$$

where Q_0 is the surface heat flow, A is the heat production, and k is the thermal conductivity. For continental rocks the onset of quartz and feldspar plasticity controls the maximum depth of seismic faulting. This transition may occur at temperatures of 300°C to 450°C [e.g., *Scholz*, 1988]. The maximum depth of brittle faulting can be approximated reorganizing the equation to

$$z = Q_0/A - \left[{Q_0}^2/A^2 - (2\,k\,\mathrm{d}T/A)\right]^{1/2}$$

where $\mathrm{d}T = T(z) - T_0$ is the temperature difference between the seafloor and temperature at depth z. We consider the 450°C isotherm as the upper temperature limit defining the maximum depth of seismogenic behavior. At the seabed, we approximate the temperature with ~0°C. *Fernàndez et al*. [1998] studied the radiogenic heat production and thermal conductivity of Iberia, providing in the Betics a heat production ranging from 1.0 to 2.7 $\mu W/m^3$ and a thermal conductivity of 1.8 to 2.8 W/m K. Following *Fullea et al*. [2010], we used a heat production and thermal conductivity of $A = 1.25\ \mu W/m^3$ and k = 2.5 W/m K, respectively. Q_0 is approximated with 120 mW/m^2 and was obtained by averaging the heat flow of the East Alboran Basin measured by *Polyak et al*. [1996]. The calculated depths for the 450°C isotherm below which no earthquakes occur in the lithosphere is ~10 km. Considering the simplicity of our calculation, this estimate fits nicely with our observation that most earthquakes in the East Alboran Basin occur shallower than 10 to 15 km with the majority rupturing at $<$10 km (Figure 2).

Approaching Morocco to the south and Spain to the north, heat flow decreases [e.g., *Fernàndez et al*., 1998], suggesting that the thickness of the seismogenic layer increases. This conclusion may explain the pattern of the historical seismicity observed in the Alboran domain and adjacent coastal areas. Thus, the largest earthquakes occurred either on land or close to the shoreline, like the 1910 Adra earthquake (MSK VIII), the 1804 Dalías earthquake (MSK IX), or the 1522 Almeria earthquake (MSK IX) [*Instituto Geográfico Nacional*, 2013, http://www.ign.es/ign/resources/sismologia/publicaciones/CatalogoGeneralIsosistas.pdf; *Keller et al*., 1995] where the 450°C isotherm tends to get deeper, and, in turn, increases the depth extent of the seismogenic zone. It is therefore reasonable to hypothesize that the lower level of seismicity in the central and eastern part of the Alboran Sea is related to a thinner seismogenic layer compared to coastal and onshore areas, reducing the size of fault planes. However, approaching the margins of the Alboran Sea the potential for earthquake hazards increases as the seismogenic layer gets thicker with lower heat flow and thicker crust.

Earthquakes in the West Alboran Basin occurring at 60 to 100 km depth cannot be crustal earthquakes. Heat flow in the western basin is ~70 mW/m^2 [*Polyak et al*., 1996] much lower than in the Eastern Basin. However, calculations suggest that any crustal seismicity is related to depth $<$25 km. We therefore favor the interpretation that intermediate depth earthquakes are related to a subducting slab hanging below the Gibraltar arc and West Alboran Basin [e.g., *Sparkman and Wortel*, 2004; *García-Castellanos and Villaseñor*, 2011; *Pedrera et al*., 2011; *Ruiz-Constán et al*., 2011].

6. Conclusions

A local deployment of 30 ocean bottom seismometers was carried out between August 2009 and January 2010 in the Alboran Sea to define the seismicity pattern in the vicinity of the African-Eurasian plate boundary where a discrete plate boundary fault zone is equivocal. The offshore deployment was supplemented by 155 seismometers installed in Spain and Morocco. In total, we observed 229 local earthquakes within the Alboran Sea and adjacent areas ranging in moment magnitude (Mw) from 0.6 to 3.6. The majority of events were in the order of Mw = 1.5 to 2.8.

We derived a minimum 1-D model from the travel time data of the local earthquakes, supporting previous suggestions that the Alboran Sea is underlain by thinned continental crust. The rift basin has an average crustal thickness of about 21 km, and its velocity structure resembles that of continental crust. Since the crust beneath and the Rif and Betic orogenic belts is ~35 km, this suggests a thinning factor of ~1.7, consistent with tectonic subsidence analysis of deep commercial wells [*Watts et al*., 1993].

Across the Alboran Sea, seismicity occurs in a 20 to 40 km wide band, roughly trending NE-SW. Seismicity is higher in the vicinity of Al Hoceima in Morocco, an area that was last affected in 2004 by a Mw = 6.3

earthquake, perhaps indicating that postseismic stresses still affect local stress patterns. Seismicity roughly outlines a complex onshore-offshore fault system connecting the city of Al Hoceima with the SW end of the Alboran Ridge [e.g., *d'Acremont et al*., 2014]. Seismic activity along the Alboran Ridge is sparse, and stress pattern are variable. However, a Mw = 3.4 earthquake to the northeast of the Alboran Ridge suggests plate convergence, mimicking the NW-SE trending compression. A cluster of earthquakes that underlie the Alboran Channel to the northeast of Alboran Island seems to be related to a set of roughly E-W trending faults imaged in the bathymetry and seismic data, supporting the interpretation of distributed deformation instead of focused deformation along a single, major plate boundary fault. Similar patterns have been observed to the southwest of Adra in Spain, where bathymetric data also show a number of NE-SW trending elongated features, which, on the basis of high-resolution seismics, would correspond to NE-SW trending active faults. Earthquakes clustering along these faults support present-day active deformation. Focal mechanisms [*Stich et al*., 2003a, 2010, and this study] support left-lateral strike-slip motion.

Seismicity and stress pattern suggest that tectonics in the Alboran domain are dominated by the convergence between Africa and Eurasia. However, a slowly westward moving or sinking slab under the western Alboran Basin may still cause back-arc extension roughly paralleling the trend of the Trans-Alboran Shear Zone.

Acknowledgments

This study is part of the TOPO-EUROPE initiative of the EUROCORES Program of the European Science Foundation (ESF). The German efforts of TOPO-MED were funded by the German Science Foundation (DFG grant GR1964/12-1). Deployment of seismic stations in Morocco and Spain were part of TOPO-IBERIA (grant CSD2006-00041). Acquisition of seismic reflection data during the RRS *Charles Darwin* cruise CD64 was funded by the National Environmental Research Council (NERC grant GR9/166). We thank the "German Instrument Pool for Amphibian Seismology (DEPAS)," hosted by the Alfred Wegener Institute Bremerhaven, for providing nine OBS operating CMG-40T sensors. Additional support came from the Spanish MICINN projects EVENT (CGL2006-12861-C02-02), ESF TopoEurope TOPOMED Project (CGL2008-03474-E/BTE), SHAKE (CGL2011-30005-C02-02), and COST Action ES1301 "FLOWS." We like to thank Captain Michael Schneider and his crew of R/V *Poseidon* cruises P389 and P393 for excellent sea-going support. Reviews of Wim Spakman and an anonymous reviewer are greatly appreciated. Figures were produced using the Generic Mapping Tools (GMT) software [*Wessel and Smith*,]. Seismological data are available on request from the first author.

References

Akoglu, A. M., Z. Cakir, M. Meghraoui, S. Belabbes, S. O. El Alami, S. Ergintav, and H. S. Akyüz (2006), The 1994–2004 Al Hoceima (Morocco) earthquake sequence: Conjugate fault ruptures deduced from InSAR, *Earth Planet. Sci. Lett.*, *252*, 467–480.

Ballesteros, M., J. Rivera, A. Muñoz, J. Acosta, A. Carbó, and E. Uchupi (2008), Alboran Basin, southern Spain—Part II: Neogene tectonic implications for the orogenic float model, *Mar. Pet. Geol.*, *25*, 75–101.

Banda, E., J. Gallart, V. Garcia-Duenas, J. J. Dañobeitia, and J. Makris (1993), Lateral variations of the crust in the Iberian Peninsula: New evidence from the Betic Cordillera, *Tectonophysics*, *221*, 53–66.

Bezada, M. J., E. D. Humphreys, D. R. Toomey, M. Harnafi, and J. M. Dávila (2013), Evidence for slab rollback in westernmost Mediterranean from improved upper mantle imaging, *Earth Planet. Sci. Lett.*, *368*, 51–60.

Blanco, M. J., and W. Spakman (1993), The *P*-wave velocity structure of the mantle below the Iberian Peninsula: Evidence for subducted lithosphere below southern Spain, *Tectonophysics*, *221*, 13–34.

Booth-Rea, G., C. R. Ranero, J. M. Martínez-Martínez, and I. Grevemeyer (2007), Crustal types and Tertiary tectonic evolution of the Alboran sea, western Mediterranean, *Geochem. Geophys. Geosyst.*, *8*, Q10005, doi:10.1029/2007GC001639.

Bourgois, J., A. Mauffret, A. Ammar, and A. Demnati (1992), Multichannel seismic data imaging of inversion tectonics of the Alboran Ridge (western Mediterranean Sea), *Geo-Mar. Lett.*, *12*, 117–122.

Bousquet, J. C. (1979), Quaternary strike-slip faults in southeastern Spain, *Tectonophysics*, *52*, 277–286.

Buforn, E., M. Bezzeghoud, A. Udías, and C. Pro (2004), Seismic sources on the Iberia-African plate boundary and their tectonic implications, *Pure Appl. Geophys.*, *16*, 623–646.

Calvert, A., F. Gómez, D. Seber, M. Barazangi, N. Jabour, A. Ibenbrahim, and A. Demnati (1997), An integrated geophysical investigation of recent seismicity in the Al-Hoceima region of North Morocco, *Bull. Seismol. Soc. Am.*, *87*, 637–651.

Calvert, A., E. Sandvol, D. Seber, M. Barazangi, S. Roecker, T. Mourabit, F. Vidal, G. Alguacil, and N. Jabour (2000), Geodynamic evolution of the lithosphere and upper mantle beneath the Alboran region of the western Mediterranean: Constraints from travel time tomography, *J. Geophys. Res.*, *105*, 10,871–10,898, doi:10.1029/2000JB900024.

Chertova, M. V., W. Spakman, T. Geenen, A. P. van den Berg, and D. J. J. Van Hinsbergen (2014), Underpinning tectonic reconstructions of the western Mediterranean region with dynamic slab evolution from 3-D numerical modeling, *J. Geophys. Res. Solid Earth*, *119*, 5876–5902, doi:10.1002/2014JB011150.

Christensen, N. I., and W. D. Mooney (1995), Seismic velocity structure and composition of the continental crust: A global view, *J. Geophys. Res.*, *100*, 9761–9788, doi:10.1029/95JB00259.

Comas, M. C., J. J. Dañobeitia, J. Alvarez-Marron, and J. I. Soto (1995), Crustal reflections and structure in the Alboran Basin. Preliminary results of the ESCI-Alboran survey, *Rev. Soc. Geol. Esp.*, *8*, 529–542.

Comas, M. C., J. P. Platt, J. I. Soto, and A. B. Watts (1999), The origin and tectonic history of the Alboran Basin: Insights from Leg 161 results, *Proc. Ocean Drill. Program Sci. Results*, *161*, 555–579.

Contreras-Reyes, E., I. Grevemeyer, A. B. Watts, E. R. Flueh, C. Peirce, S. Moeller, and C. Papenberg (2011), Deep seismic structure of the Tonga subduction zone: Implications for mantle hydration, tectonic erosion, and arc magmatism, *J. Geophys. Res.*, *116*, B10103, doi:10.1029/2011JB008434.

d'Acremont, E., et al. (2014), High-resolution imagery of active faulting offshore Al Hoceima, Northern Morocco, *Tectonophysics*, *632*, 160–166.

De Larouzière, F., J. deBolze, P. Bordet, J. Hernandez, C. Montenat, and P. Ott d'Estevou (1988), The Betic segment of the lithospheric Trans-Alboran shear zone during the late Miocene, *Tectonophysics*, *152*, 41–52.

De Mets, C., R. G. Gordon, and D. F. Argus (2010), Geologically current plate motions, *Geophys. J. Int.*, *181*, 1–80, doi:10.1111/j.1365-246X.2009.04491.x.

Doser, D. I., and H. Kanamori (1986), Depth of seismicity in the Imperial Valley region (1977–1983) and its relationship to heat flow, crustal structure, and the October 15, 1979, earthquake, *J. Geophys. Res.*, *91*, 675–688, doi:10.1029/JB091iB01p00675.

Duggen, S., K. Hoernle, P. van den Bogaard, L. Ruepke, and J. Phipps Morgan (2003), Deep roots of the Messinian salinity crisis, *Nature*, *422*, 602–606.

Duggen, S., K. Hoernle, P. van den Bogaard, and C. Harris (2004), The role of subduction in forming the western Mediterranean and causing the Messinian Salinity Crisis, *Earth Planet. Sci. Lett.*, *218*, 91–108.

El Moudnib, L. E., et al. (2015), Crustal structure of the Betic–Rif system, western Mediterranean, from local earthquake tomography, *Tectonophysics*, *643*, 94–105, doi:10.1016/j.tecto.2014.12.015.

Faccenna, C., T. W. Becker, F. Pio-Lucente, L. Jolivet, and F. Rosseti (2001), History of subduction and back-arc extension in the Central Mediterranean, *Geophys. J. Int.*, *145*, 809–820.

Fernàndez, M., I. Marzán, A. Correia, and E. Ramalho (1998), Heat flow, heat production, and lithospheric thermal regime in the Iberian Peninsula, *Tectonophysics*, *291*, 29–53.
Fullea, J., M. Fernàndez, J. C. Afonso, J. Vergés, and H. Zeyen (2010), The structure and evolution of the lithosphere–asthenosphere boundary beneath the Atlantic–Mediterranean Transition Region, *Lithos*, *120*, 74–95, doi:10.1016/j.lithos.2010.03.003.
García-Castellanos, D., and A. Villasenor (2011), Messinian salinity crisis regulated by competing tectonics and erosion at the Gibraltar arc, *Nature*, *480*, 359–363.
Gràcia, E., J. J. Dañobeitia, J. Vergés, and P. A. R. S. I. F. A. L. Team (2003), Mapping active faults offshore Portugal (36N–38N): Implications for seismic hazard along the southwest Iberian margin, *Geology*, *31*, 83–86.
Gràcia, E., R. Pallàs, J. I. Soto, M. Comas, X. Moreno, E. Masana, P. Santanach, S. Diez, M. García, and J. J. Dañobeitia (2006), Active faulting offshore SE Spain (Alboran Sea): Implications for earthquake hazard assessment in the Southern Iberia Margin, *Earth Planet. Sci. Lett.*, *241*, 734–749.
Gràcia, E., et al. (2012), Acoustic and seismic imaging of the Adra Fault (NE Alboran Sea): In search of the source of the 1910 Adra earthquake, *Nat. Hazards Earth Syst. Sci.*, *12*, 3255–3267.
Grevemeyer, I., N. Kaul, and A. Kopf (2009), Heat flow anomalies in the Gulf of Cadiz and off Cape San Vicente, Portugal, *Mar. Pet. Geol.*, *26*, 795–804, doi:10.1016/j.marpetgeo.2008.08.006.
Gutscher, M.-A. (2004), What caused the great Lisbon earthquake?, *Science*, *305*, 1247–1248.
Hardebeck, J. L., and P. M. Shearer (2002), A new method for determining first-motion focal mechanisms, *Bull. Seismol. Soc. Am.*, *92*, 2264–2276, doi:10.1785/0120010200.
Havskov, J., and L. Ottemöller (2000), SEISAN earthquake analysis software, *Seismol. Res. Lett.*, *70*, 532–534.
Heuret, A., and S. Lallemand (2005), Plate motions, slab dynamics and back-arc deformation, *Phys. Earth Planet. Inter.*, *149*, 31–51.
Keller, J. V. A., S. H. Hall, C. J. Dart, and K. R. McClay (1995), The geometry and evolution of a transpressional strike-slip system: The Carboneras fault, SE Spain, *J. Geol. Soc. London*, *152*, 339–351.
Kissling, E. (1988), Geotomography with local earthquake data, *Rev. Geophys.*, *26*, 659–698, doi:10.1029/RG026i004p00659.
Kissling, E., W. L. Ellsworth, D. Eberhart-Phillips, and U. Kadolfer (1994), Initial reference models in local earthquake tomography, *J. Geophys. Res.*, *99*, 19,635–19,646, doi:10.1029/93JB03138.
Koulali, A. D., A. Ouazar, R. W. Tahayt, P. King, R. E. Vernant, S. Reilinger, T. McClusky, J. M. D. Mourabit, and N. Amraoui (2011), New GPS constraints on active deformation along the Africa-Iberia boundary, *Earth Planet. Sci. Lett.*, *308*, 211–217.
Lomax, A., A. J. Virieux, P. Volant, and C. Berge (2000), Probabilistic earthquake location in 3D and layered models: Introduction of a Metropolis-Gibbs method and comparison with linear locations, in *Advances in Seismic Event Location*, edited by C. H. Thurber and N. Rabinowitz, pp. 101–134, Kluwer, Amsterdam.
Marín-Lechado, C., J. Galindo-Zaldívar, L. R. Rodríguez-Fernández, I. Serrano, and A. Pedrera (2005), Active faults, seismicity and stresses in an internal boundary of a tectonic arc (Campo de Dalias and Nijar, southeastern Betic Cordilleras, Spain), *Tectonophysics*, *396*, 81–96.
Martínez-García, P., J. I. Soto, and M. Comas (2011), Recent structures in the Alboran Ridge and Yusuf fault zones based on swath bathymetry and sub-bottom profiling: Evidence of active tectonics, *Geo. Mar. Lett.*, *31*, 19–36.
Martínez-García, P., M. Comas, J. I. Soto, L. Lonergan, and A. B. Watts (2013), Strike-slip tectonics and basin inversion in the Western Mediterranean: The Post-Messinian evolution of the Alboran Sea, *Basin Res.*, *25*, 1–27, doi:10.1111/bre.120005.
Mauffret, A., D. Frizon de Lamotte, S. Lallemant, C. Gorini, and A. Maillard (2004), E-W opening of the Algerian Basin (western Mediterranean), *Terra Nova*, *16*, 257–264, doi:10.1111/j.1365-3121.2004.00559.x.
Mauffret, A., A. Ammar, C. Gorini, and H. Jabour (2007), The Alboran Sea (Western Mediterranean) revisited with a view from the Moroccan Margin, *Terra Nova*, *19*, 195–203, doi:10.1111/j.1365-3121.2007.00734.x.
McClusky, S., R. Reilinger, S. Mahmoud, D. Ben Sari, and A. Tealeb (2003), GPS constraints on Africa (Nubia) and Arabia plate motions, *Geophys. J. Int.*, *155*(1), 126–138, doi:10.1046/j.1365-246X.2003.02023.x.
MEDIMAP Group (2008), Morpho-bathymetry of the Mediterranean Sea, CIESM/IFREMER Spec. Publ., Scale: 1/3.000.000.
Meghraoui, M., and S. Pondrelli (2012), Active faulting and transpression tectonics along the plate boundary in North Africa, *Ann. Geophys.*, *55*(5), 955–967, doi:10.4401/ag-4970.
Muñoz, A., M. Ballesteros, I. Montoya, J. Rivera, J. Acosta, and E. Uchupi (2008), Alboran Basin, southern Spain—Part I: Geomorphology, *Mar. Pet. Geol.*, *25*, 59–73.
Ottemöller, L., and J. Havskov (2003), Moment magnitude determination for local and regional earthquakes based on source spectra, *Bull. Seismol. Soc. Am.*, *93*, 203–214.
Pedrera, A., et al. (2011), Is there an active subduction beneath the Gibraltar orogenic arc? Constraints from Pliocene to present-day stress field, *J. Geodyn.*, *52*, 83–96, doi:10.1016/j.jog.2010.12.003.
Perouse, E., P. Vernant, J. Chery, R. Rellinger, and S. McClusky (2010), Active surface deformation and sub-lithospheric processes in the western Mediterranean constrained by numerical models, *Geology*, *38*, 823–826.
Platt, J. P., and R. L. M. Vissers (1989), Extensional collapse of thickened continental lithosphere: A working hypothesis for the Alboran Sea and Gibraltar Arc, *Geology*, *17*, 540–543.
Polyak, B. G., et al. (1996), Heat-flow in the Alboran Sea, western Mediterranean, *Tectonophysics*, *263*(1–4), 191–218.
Rebai, S., H. Philip, and A. Taboada (1992), Modern tectonic stress field in the Mediterranean region; evidence for variation in stress direction at different scales, *Geophys. J. Int.*, *110*, 106–140.
Reicherter, K., and C. Hübscher (2007), Evidence for a seafloor rupture of the Carboneras Fault (southern Spain): Relation to the 1522 Almeria earthquake?, *J. Seismol.*, *11*, 15–26.
Royden, L. H. (1993), Evolution of retreating subduction boundaries formed during continental collision, *Tectonics*, *12*, 629–638, doi:10.1029/92TC02641.
Ruiz-Constán, A., J. Galindo-Zaldívar, A. Pedrera, B. Célérier, and C. Marín-Lechado (2011), Stress distribution at the transition from subduction to continental collision (northwestern and central Betic Cordillera), *Geochem. Geophys. Geosyst.*, *12*, Q12002, doi:10.1029/2011GC003824.
Sanz de Galdeano, C. (1990), Geologic evolution of the Betic Cordilleras in the Western Mediterranean, Miocene to present, *Tectonophysics*, *172*, 107–119.
Scholz, C. H. (1988), The brittle-plastic transition and the depth of seismic faulting, *Geologische Rundschau*, *77*, 319–328.
Snoke, J. A., J. W. Munsey, A. G. Teague, and G. A. Bollinger (1984), A program for focal mechanism determination by combined use of polarity and SV-P amplitude ratio data, *Earthquake Notes*, *55*.
Sparkman, W., and R. Wortel (2004), A tomographic view on Western Mediterranean Geodynamics, in *The TRANSMED Atlas. The Mediterranean Region From Crust to Mantle*, edited by W. Cavazza et al., pp. 31–52, Springer, Berlin.

Stich, D., C. J. Ammon, and J. Morales (2003a), Moment tensor solutions for small and moderate earthquakes in the Ibero-Maghreb region, *J. Geophys. Res.*, *108*, 2148, doi:10.1029/2002JB002057.

Stich, D., J. Batlló, J. Morales, R. Macia, and S. Dineva (2003b), Source parameters of the Mw = 6.1 1910 Adra earthquake (southern Spain), *Geophys. J. Int.*, *155*, 539–546.

Stich, D., F. Mancilla, D. Baumont, and J. Morales (2005), Source analysis of the Mw 6.3 2004 Al Hoceima earthquake [Morocco] using regional apparent source time functions, *J. Geophys. Res.*, *110*, B06306, doi:10.1029/2004JB003366.

Stich, D., E. Serpelloni, F. Mancilla, and J. Morales (2006), Kinematics of the Iberia–Maghreb plate contact from seismic moment tensors and GPS observations, *Tectonophysics*, *426*, 295–317.

Stich, D., R. Martin, and J. Morales (2010), Moment tensor inversion for Iberia-Maghreb earthquakes 2005–2008, *Tectonophysics*, *483*, 390–398.

Tanaka, A., and Y. Ishikawa (2002), Temperature distribution and focal depth in the crust of northeastern Japan, *Earth Planets Space*, *54*, 1109–1113.

van Hinsbergen, D. J. J., R. L. M. Vissers, and W. Spakman (2014), Origin and consequences of western Mediterranean subduction, rollback, and slab segmentation, *Tectonics*, *33*, 393–419, doi:10.1002/tect.20125.

Watts, A. B., J. P. Platt, and P. Buhl (1993), Tectonic evolution of the Alboran Sea basin, *Basin Res.*, *5*, 153–177.

Wessel, P., and W. H. F. Smith (1998), New, improved version of Generic Mapping Tools released, *Eos Trans. AGU*, *79*, 579.